NASA TM X-8

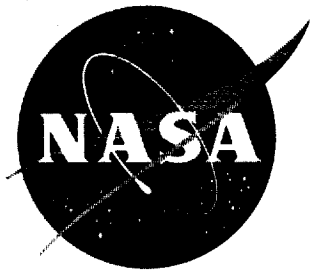

TECHNICAL MEMORANDUM
X - 8

AERODYNAMIC CHARACTERISTICS AT MACH NUMBERS FROM 1.6 TO 2.8 OF 74° SWEPT ARROW WINGS WITH AND WITHOUT CAMBER AND TWIST

By Dennis F. Hasson, Ann B. Fichter, and Norman Wong

Langley Research Center
Langley Field, Va.

Declassified September 1, 1961

NATIONAL AERONAUTICS AND SPACE ADMINISTRATION

WASHINGTON September 1959

NATIONAL AERONAUTICS AND SPACE ADMINISTRATION

TECHNICAL MEMORANDUM X-8

AERODYNAMIC CHARACTERISTICS AT MACH NUMBERS FROM 1.6 TO 2.8 OF 74° SWEPT ARROW WINGS WITH AND WITHOUT CAMBER AND TWIST*

By Dennis F. Hasson, Ann B. Fichter, and Norman Wong

SUMMARY

An investigation has been conducted to determine the lift, drag, and pitching-moment characteristics of a cambered and twisted arrow wing and an uncambered and untwisted arrow wing. The cambered and twisted wing was designed to give a high value of maximum lift-drag ratio at a lift coefficient of 0.1 and at a Mach number of 2.50. Each wing had a leading-edge sweep of 74°, an aspect ratio of 1.6, a taper ratio of 0, and a notch ratio of 0.714. A 3-percent-streamwise biconvex thickness distribution was centered on the mean camber surface of both wings.

Tests were conducted at Mach numbers from 1.6 to 2.8 through a range of angle of attack from -6° to 14°. The Reynolds number based on mean aerodynamic chord was 5.0×10^6 for all tests.

The maximum lift-drag ratio at the design Mach number for the cambered and twisted wing was 7.85 and, thus, was below the theoretically predicted value of 9.10. In addition, the cambered and twisted wing had only slightly higher values of maximum lift-drag ratio throughout the test Mach number range than the uncambered and untwisted wing.

With the moment reference centers at 0.565 wing mean aerodynamic chord, both wings were slightly unstable longitudinally at low lift coefficients. For lift coefficients greater than about 0.1, the instability became more marked. These characteristics were obtained at all Mach numbers at which tests were made.

INTRODUCTION

Current interest in the development of airplane configurations having long-range capabilities at supersonic speeds has resulted in extensive investigations of arrangements designed to produce high values of maximum lift-drag ratio. One approach to this problem has been the utilization of camber and twist because of the substantial gains indicated by theory. One such configuration (ref. 1), designed for a Mach number of 3.00 incorporated a 75° swept, cambered and twisted arrow wing with a subsonic leading edge and was designed to give minimum induced drag at a lift coefficient of 0.1. At the design Mach number of 3.00, the experimental maximum lift-drag ratio, however, was below the theoretically predicted one by about 15 percent. This difference in experimental maximum lift-drag ratio was attributed to the existence of supercritical flow (Mach number > 1 perpendicular to the leading edge) on the upper surface of the wing which produced large regions of flow separation. Insufficient sweep for the design Mach number is a probable explanation for the existence of this critical flow condition.

L 3 6 9

It was, therefore, of interest to utilize the foregoing information in designing a cambered and twisted arrow wing which would be expected to give better correlation with theory. Thus, a 74° swept, cambered and twisted arrow wing was designed[1] to give minimum induced drag at a lift coefficient of 0.1 at a Mach number of 2.50, and at this lower Mach number the sweep limitations are less severe.

In the present design, the induced velocities over a large portion of the wing span were reduced from those existing on the wing of reference 1. However, the theoretical pressure coefficients in the vicinity of the leading edge correspond to induced Mach numbers perpendicular to the leading edge which are still in excess of sonic velocity. This procedure was followed because it was assumed that a low supersonic Mach number component was allowable before a shock of sufficient strength to cause separation and drastic changes in the loading over the wing would be produced.

The cambered and twisted wing just discussed and an uncambered and untwisted wing of the same plan form were tested in the Langley Unitary Plan wind tunnel at Mach numbers from 1.6 to 2.8. A 3-percent-thick biconvex section referenced to the camber surface was employed in both cases.

---

[1]The cambered and twisted wing reported herein was designed at The Martin Company (Baltimore) using the method of reference 2.

SYMBOLS

The force and moment-coefficient data are presented about the stability axes system. The reference centers and reference planes are shown in figure 1.

b	wing span, in.
$\bar{c}$	wing mean aerodynamic chord, 15.492 in.
c	local chord, in.
C_D'	drag coefficient, $\frac{\text{Drag}}{qS}$
$C_{D,b}'$	base drag coefficient, $\frac{\text{Base drag}}{qS}$
C_L	lift coefficient, $\frac{\text{Lift}}{qS}$
C_m	pitching-moment coefficient, $\frac{\text{Pitching moment}}{qS\bar{c}}$
C_p	pressure coefficient, $\frac{p_l - p}{q}$
C_{L_α}	lift-curve slope, per deg
L/D	lift-drag ratio
$\frac{\partial C_D'}{\partial C_L^2}$	drag-due-to-lift factor, $\frac{C_D' \text{ at } (L/D)_{max} - C_{D,min}' \text{ for flat wing}}{C_L^2 \text{ for } (L/D)_{max}}$
M	free-stream Mach number
p	free-stream static pressure, lb/sq ft
p_l	local static pressure, lb/sq ft
q	free-stream dynamic pressure, $0.7pM^2$, lb/sq ft
R	Reynolds number, based on $\bar{c}$, $\frac{\rho V \bar{c}}{\mu}$

S	total wing area, 1.500 sq ft
V	free-stream velocity
α	angle of attack of reference plane, deg
α_f	flow angle (positive for upflow), deg
μ	free-stream viscosity, slugs/ft-sec
ρ	free-stream density, slugs/cu ft

Subscripts:

max	maximum
min	minimum

MODELS AND APPARATUS

Dimensional details and photographs of the models tested are presented in figures 1 and 2, and the geometric characteristics are given in table I. The ordinates of the mean camber surface for the cambered and twisted wing, as determined by the method of reference 2, are given in table II.

A 3-percent-streamwise biconvex thickness distribution was centered on the mean camber surface given in table II. The theoretical pressure distributions corresponding to the cambered and twisted wing at the design conditions are given in figure 3. The wing without camber and twist had 3-percent-streamwise biconvex sections and is referred to hereafter as the flat wing.

In order to provide a balance housing on the models, it was necessary to add small cone-cylinder bodies. The cones originated at the wing apex and had an included angle of 9°. The body for the flat wing was placed on the wing center line, and the body for the cambered and twisted wing was placed below the wing with the cone tip faired into the lower surface of the wing.

Forces and moments on the model were measured by means of a six-component internal strain-gage balance. This balance was attached, by means of a sting, to the tunnel central support system.

The tests were conducted in the low Mach number test section of the Langley Unitary Plan wind tunnel, which is a variable-pressure continuous-flow tunnel. The test section is 4 feet square and approximately 7 feet

in length and is equipped with an asymmetric sliding-block type of nozzle which allows a continuous variation of Mach numbers from 1.57 to 2.87.

TESTS

The tests were conducted at the following conditions:

	Condition 1	Condition 2	Condition 3	Condition 4	Condition 5	Condition 6
Mach number	1.60	2.02	2.36	2.50	2.65	2.80
Stagnation pressure, lb/sq in. abs . . .	14.5	17.0	21.2	22.8	24.7	26.7
Dynamic pressure, lb/sq ft	880	865	867	840	811	778
Stagnation temperature, ^{o}F	125	125	150	150	150	150
Reynolds number (based on $\bar{c}$) . . .	5×10^6	5×10^6	5×10^6	5×10^6	5×10^6	5×10^6
Dewpoint, ^{o}F	<-30	<-30	<-30	<-30	<-30	<-30
Angle-of-attack range, deg	-6 to 14	-6 to 14	-6 to 14	-6 to 14	-6 to 14	-6 to 14
Transition	Fixed	Fixed	Fixed	Fixed	Fixed	Fixed

The transition strips consisted of bands of sand 1/32 inch wide applied at 10 percent of the local streamwise chord on the wing, with a density of 100 grains per square inch. The grain size was 0.009 inch to 0.011 inch. The only natural-transition test was made on the cambered and twisted wing for the flow-visualization tests.

The flow-visualization technique utilized a fluorescent oil painted on the wing surface. A description of this technique is given in reference 3. The photographs (fig. 4) of the upper surface of the cambered and twisted wing were made with the tunnel in operation and indicate areas of attached and separated flow as well as the airflow direction at the surface. The model was translated forward and rearward in the test section in order to obtain photographic coverage of the wing, and the resulting photographs were pieced together to form the composite photograph.

CORRECTIONS AND ACCURACY

The maximum deviation of local Mach number in the part of the tunnel occupied by the model is ± 0.015 from the average value given. The present gradients are sufficiently small that no buoyancy correction is required.

The average angularity of the flow in the region of the model was determined by adjusting the zero-lift angle-of-attack value for the flat-wing model to a value of zero, and the angles of attack were corrected accordingly. The flow angles used for the tests are as follows:

M	α_f, deg
1.60	0.3
2.02	.9
2.36	1.2
2.50	.9
2.65	.5
2.80	.1

The angles of attack have also been corrected for balance-sting deflection. The data have been adjusted to the condition of free-stream static pressure on the model base.

Based upon balance accuracy and repeatability of data, it is estimated that the coefficients are accurate within the following limits:

C_L	±0.004
C'_D	±0.0005
$C'_{D,b}$	±0.0005
C_m	±0.001
α, deg	±0.1

PRESENTATION OF RESULTS

The results of this investigation are presented in the following figures:

DISCUSSION

Performance

At the design Mach number of 2.50, the experimental maximum lift-drag ratio for the cambered and twisted wing was 7.85, as compared with a theoretically predicted value of 9.10. (This value was obtained from theoretical calculations furnished Langley by the Martin Company.) At the Mach number of 2.50, the experimental value for the flat wing was 7.75. A brief discussion of possible explanations of these results follows and the results at off-design Mach numbers for both wings are given.

In figure 8(d), a comparison of the experimental and theoretical lift and drag characteristics can be made at the design Mach number of 2.50. The theoretical lift-curve slope and value for minimum drag are seen to be in fair agreement with the experimental values. An examination of the drag polars, however, shows the drag at any given lift coefficient beyond C_L for $C_{D,min}'$ to be higher for the experimental values, as compared with the theoretical values. This result is reflected in a comparison of the drag-due-to-lift factors $\partial C_D'/\partial C_L^2$ which were 0.60 and 0.42 for experiment and theory, respectively (fig. 9). These higher values of experimental drag could be associated with shock formation on the wing surface. Such a shock, since it is not included in the theory, would produce higher drag values than anticipated. The photographs of flow over the upper surface of the wing for fixed transition (fig. 4) and a lift coefficient of about 0.15 tend to confirm this conjecture. A shock and attendant flow separation are seen in the vicinity of the tips, and this is the same region where large local pressure coefficients (that is, high induced Mach numbers) are predicted by the theoretical estimates (fig. 3). The pitching-moment curves (fig. 8(d)) provide an additional indication of the flow separation at the tips because a definite destabilizing break in the pitching-moment curves occurs at a lift coefficient slightly below that for the flow picture. This fact indicates forward movement of the center of pressure; that is, a loss of lift at the tips. With regard to these effects, it is probable that if the wing had been

designed to keep the pressures along the leading edge in the vicinity of the tips at or below the values for the inboard sections, the shocks and separation would have been minimized or avoided.

The values of maximum lift-drag ratios throughout the test Mach number range for the cambered and twisted wing are only slightly higher than those for the flat wing (fig. 10).

In general, both wings showed the usual decrease in maximum lift-drag ratio with increasing Mach number. The values went from 8.40 and 8.10 at $M = 1.60$ to 7.35 and 7.30 at $M = 2.80$ for the cambered and twisted wing and for the flat wing, respectively. The values of $\partial C_D'/\partial C_L^2$ for both wings (fig. 9) were lower than the values of $1/C_{L_\alpha}$ (which correspond to the case of no leading-edge suction) throughout the test Mach number range. Hence, it may be concluded that both wings realized some so-called leading-edge suction.

A comparison of the cambered and twisted wings of the present investigation and those of reference 1 is given in figure 11. The new wing designed for a Mach number of 2.50 has slightly higher maximum lift-drag ratios in a comparable Mach number range probably because of the slightly lower minimum drag values for the wing of the present investigation. The difference in $(L/D)_{max}$ between theory and experiment for the wing of this present investigation is not as great as a straight-line extrapolation to a Mach number of 3.00 of the $(L/D)_{max}$ curve would indicate for the wing of reference 1. The decrease in the velocity component normal to the leading edge and the reduced thickness of the new wing thus seem to be in a direction for attaining the theoretically predicted values.

Longitudinal Stability

Examination of the pitching-moment curves (fig. 8) shows the cambered and twisted wing develops positive trimming moments throughout the lift-coefficient range of the tests. This effect is favorable, since for some static margin (that is, negative $\partial C_m/\partial C_L$) the wing would trim at or near the lift coefficient for $(L/D)_{max}$. Thus, there would be no loss in $(L/D)_{max}$ due to trimming the wing.

With the moment reference centers at $0.\overline{65}\bar{c}$, both wings were slightly unstable longitudinally at low lift coefficients and at all test Mach numbers (fig. 8). Furthermore, for lift coefficients greater than about 0.1, the instability became more marked. These instabilities are associated with the previously mentioned flow separation on the wing tips.

The location of the aerodynamic center varied from $0.555\bar{c}$ to $0.520\bar{c}$ for the cambered and twisted wing and from $0.560\bar{c}$ to $0.530\bar{c}$ for the flat wing in the Mach number range from 1.60 to 2.80 (fig. 10).

CONCLUDING REMARKS

At the design Mach number of 2.50, the experimental lift-drag ratio for the cambered and twisted arrow wing was 7.85, as compared with a theoretically predicted value of 9.10. This discrepancy was attributed to the existence of shock formation and attendant flow separation on the upper surface of the wing in the region of the tips. Thus, it is possible that a reduction in the pressures in the vicinity of the leading edge (and, consequently, the induced Mach numbers over the wing) will result in reduced separation and better correlation between theory and experiment.

In the present investigation, the cambered and twisted wing had only slightly higher values of maximum lift-drag ratio throughout the test Mach number range than did the flat wing. Both wings exhibited pitch-up tendencies at the design lift coefficient throughout the test Mach number range.

Langley Research Center,
National Aeronautics and Space Administration,
Langley Field, Va., February 10, 1959.

REFERENCES

1. Hallissy, Joseph M., Jr., and Hasson, Dennis F.: Aerodynamic Characteristics at Mach Numbers 2.36 and 2.87 of an Airplane Configuration Having a Cambered Arrow Wing With a 75° Swept Leading Edge. NACA RM L58E21, 1958.

2. Ginzel, I., and Multhopp, H.: Wings With Minimum Induced Drag in Supersonic Flow. Eng. Rep. No. 9937-M, The Glenn L. Martin Co., Aug. 1957.

3. Loving, Donald L., and Katzoff, S.: The Fluorescent-Oil Film Method and Other Techniques for Boundary-Layer Flow Visualization. NASA MEMO 3-17-59L, 1959.

70	-.0227	-.0220	-.0202	-.0178	-.0159	-.0146	-.0138	-.0132	-.0138	-.0129
75	-.0269	-.0269	-.0250	-.0221	-.0197	-.0182	-.0170	-.0162	-.0166	-.0155
80	-.0306	-.0314	-.0294	-.0260	-.0233	-.0214	-.0201	-.0189	-.0191	-.0176
85	-.0336	-.0355	-.0335	-.0296	-.0266	-.0244	-.0227	-.0211	-.0211	-.0194

10

TABLE I.- GEOMETRIC CHARACTERISTICS OF MODELS

12

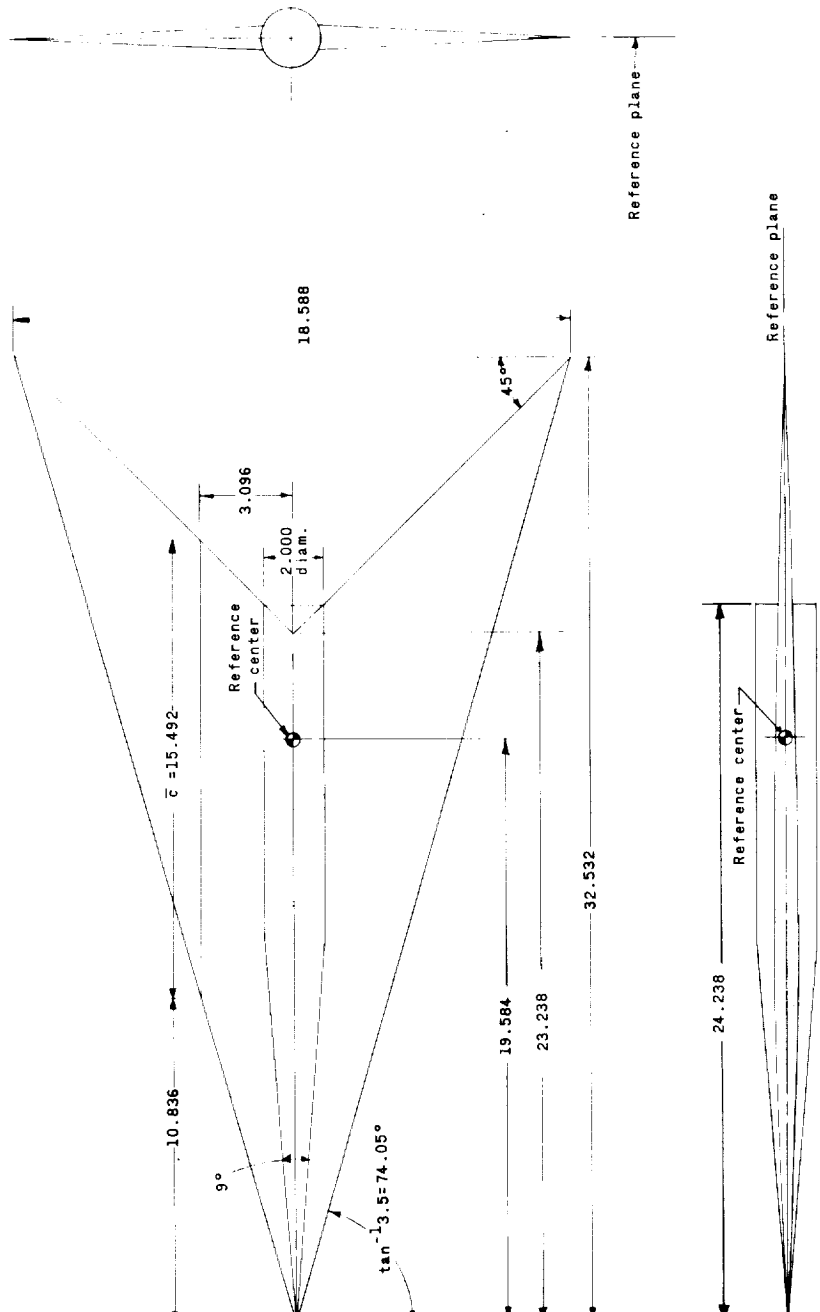

(a) Three-view drawing of flat wing.

Figure 1.- Model drawings. Dimensions are in inches unless otherwise noted.

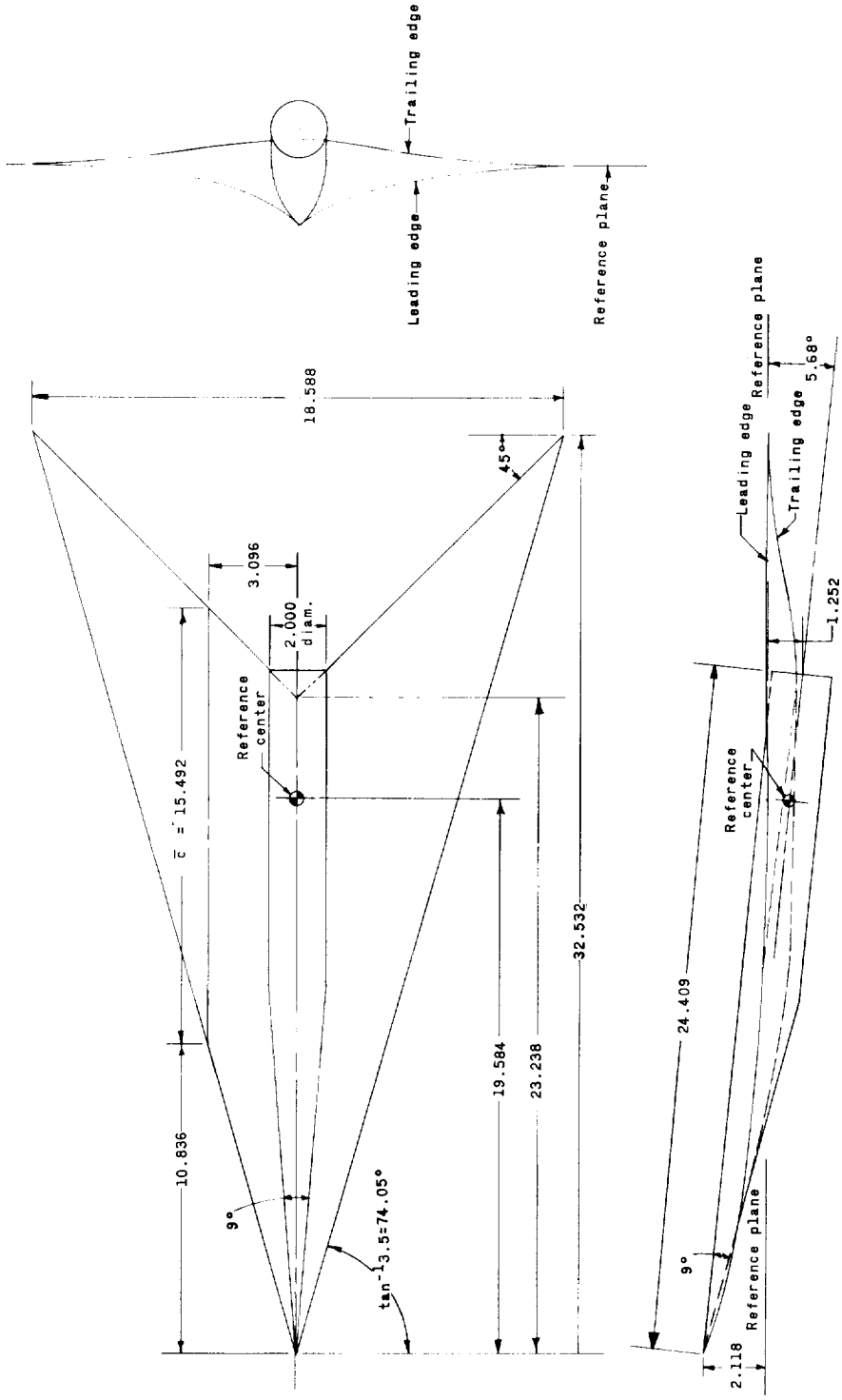

(b) Three-view drawing of cambered and twisted wing.

Figure 1.- Concluded.

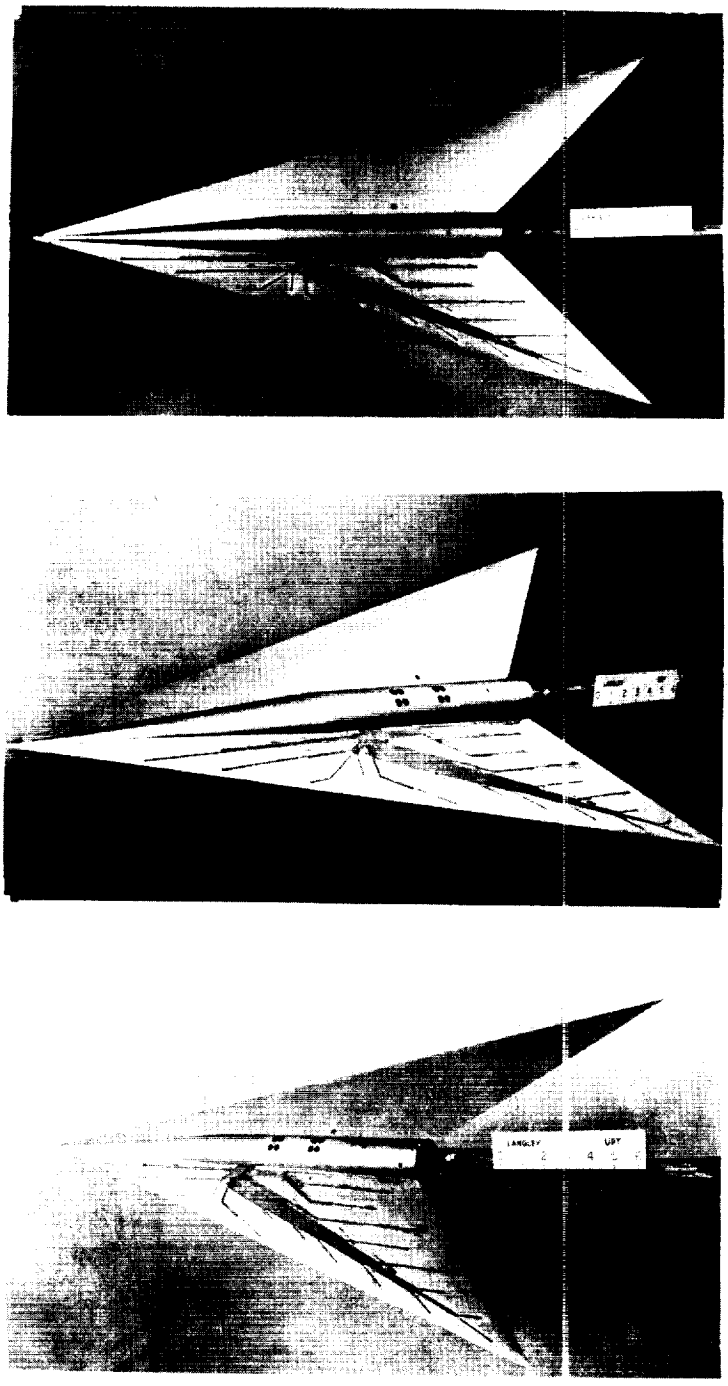

(a) Flat wing. L-59-208

Figure 2.- Photographs of the arrow-wing models.

L-369

(b) Cambered and twisted wing. L-59-209

Figure 2.- Concluded.

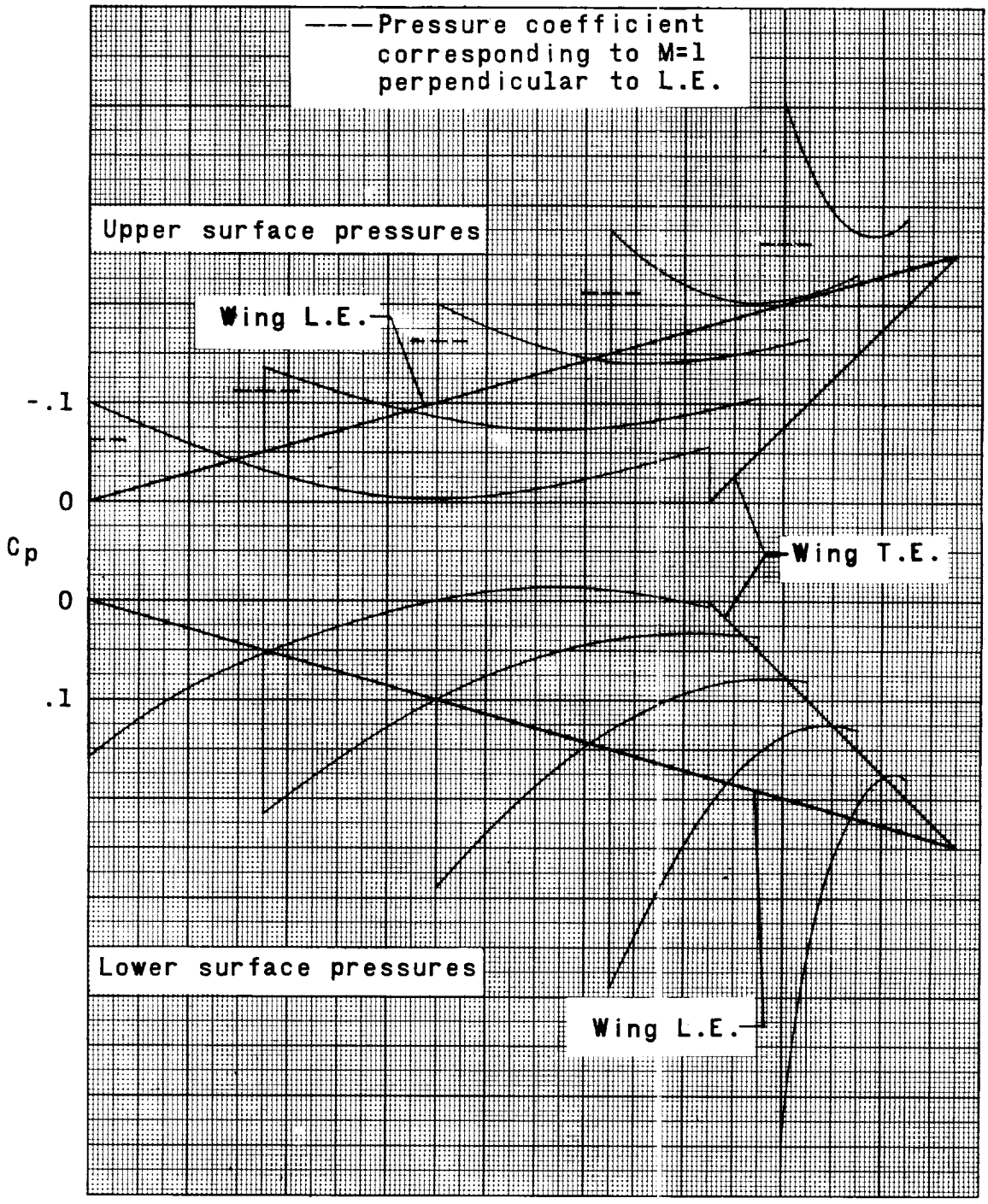

Figure 3.- Estimated pressure distributions for the cambered and twisted arrow-wing model. M = 2.50; C_L = 0.1.

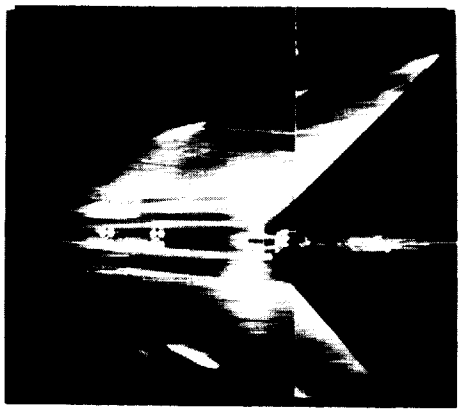

$C_L \approx 0$

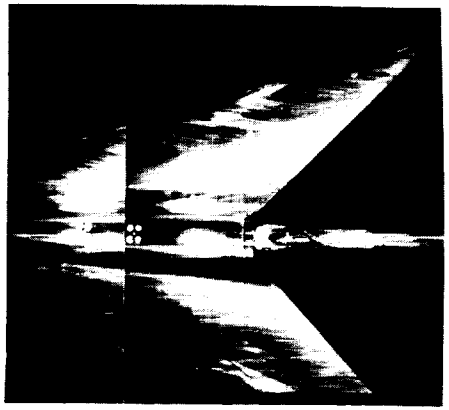

$C_L \approx 0$

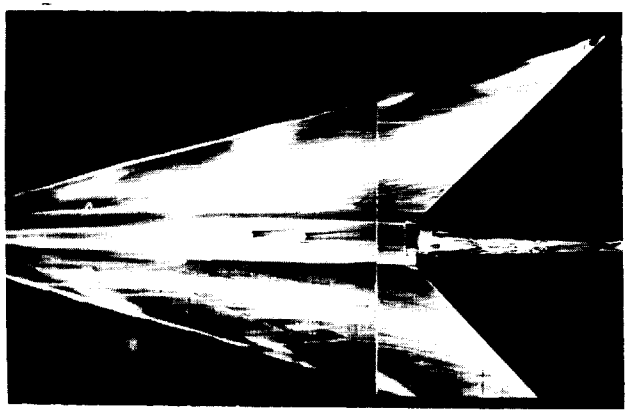

$C_L \approx .15$

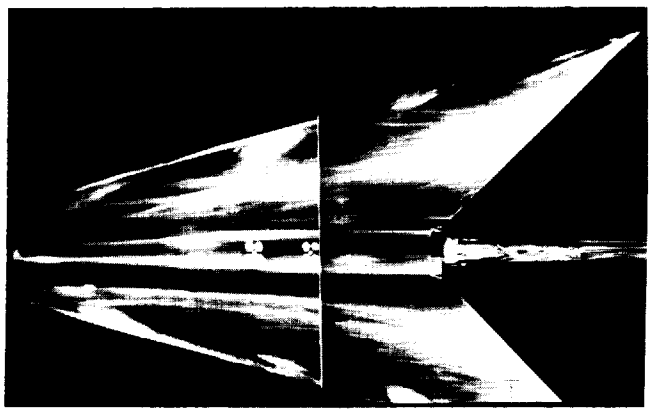

$C_L \approx .15$

(a) Transition free.

(b) Transition fixed.

L-59-210

Figure 4.- Oil-flow photographs of the cambered and twisted arrow-wing model. $M = 2.50$; $R = 5 \times 10^6$.

$C_L \approx .025$

$C_L \approx .025$

$C_L \approx .165$

$C_L \approx .140$

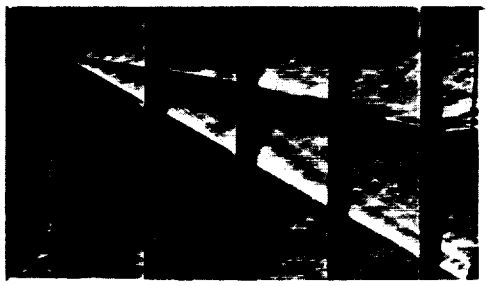

$C_L \approx .345$

$C_L \approx .260$

(a) Flat wing.

L-59-211

Figure 5.- Typical schlieren photographs of the arrow-wing models. M = 2.50.

L-369

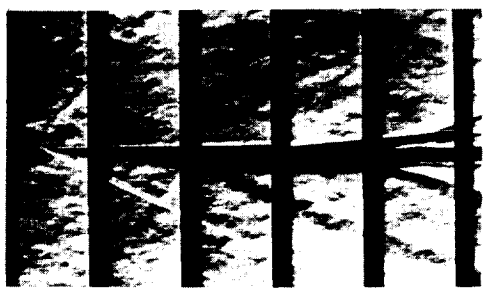

$C_L \approx 0$

$C_L \approx 0$

$C_L \approx .125$

$C_L \approx .140$

$C_L \approx .303$

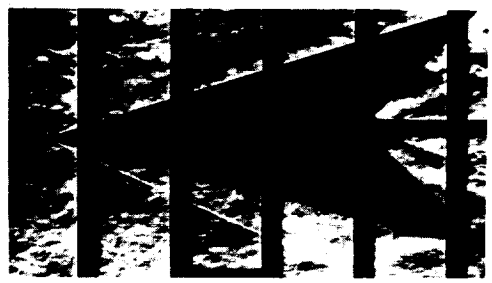

$C_L \approx .218$

(b) Cambered and twisted wing. L-59-212

Figure 5.- Concluded.

L-369

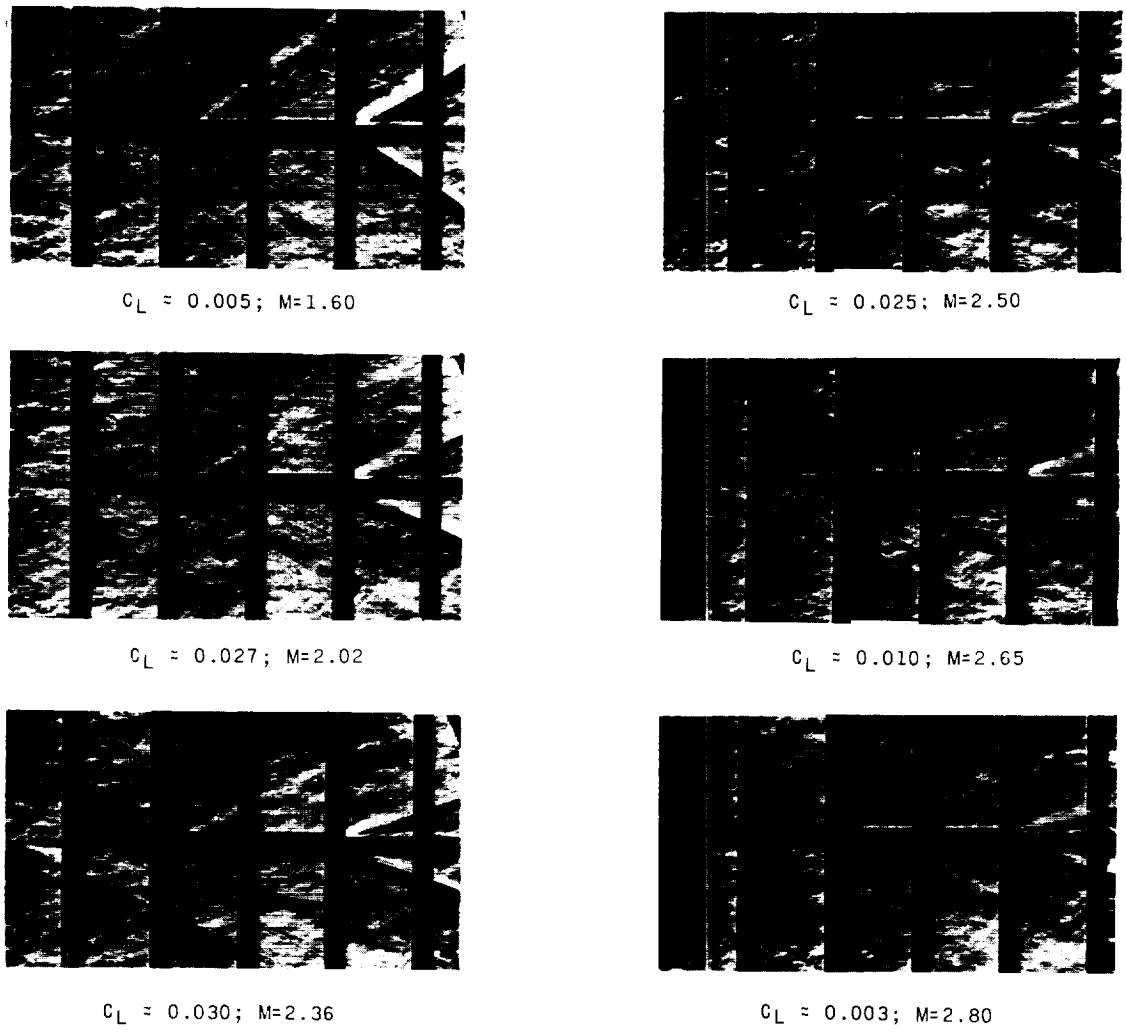

(a) Flat wing.

L-59-213

Figure 6.- Typical schlieren photographs of the arrow-wing models at various Mach numbers.

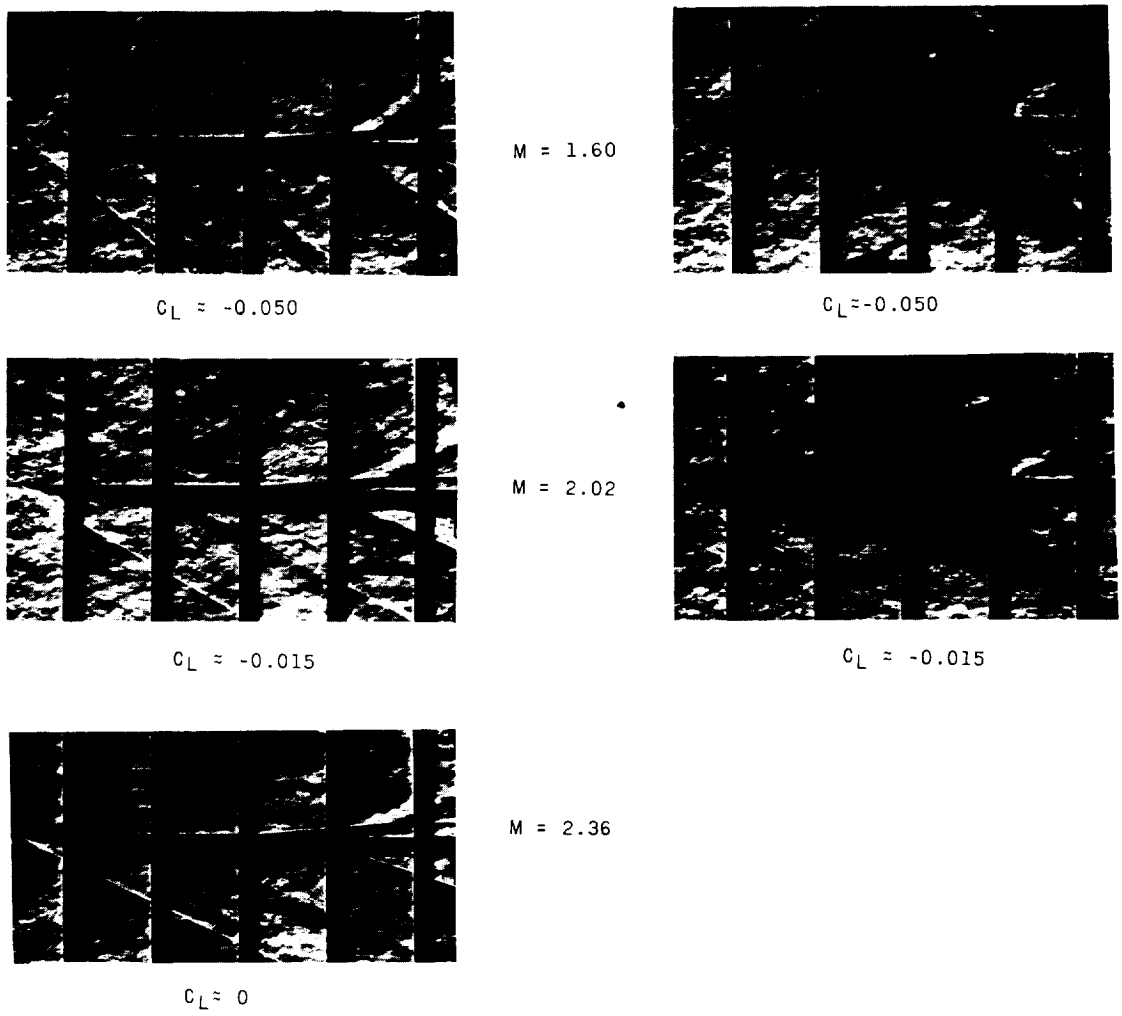

(b) Cambered and twisted wing. L-59-214

Figure 6.- Continued.

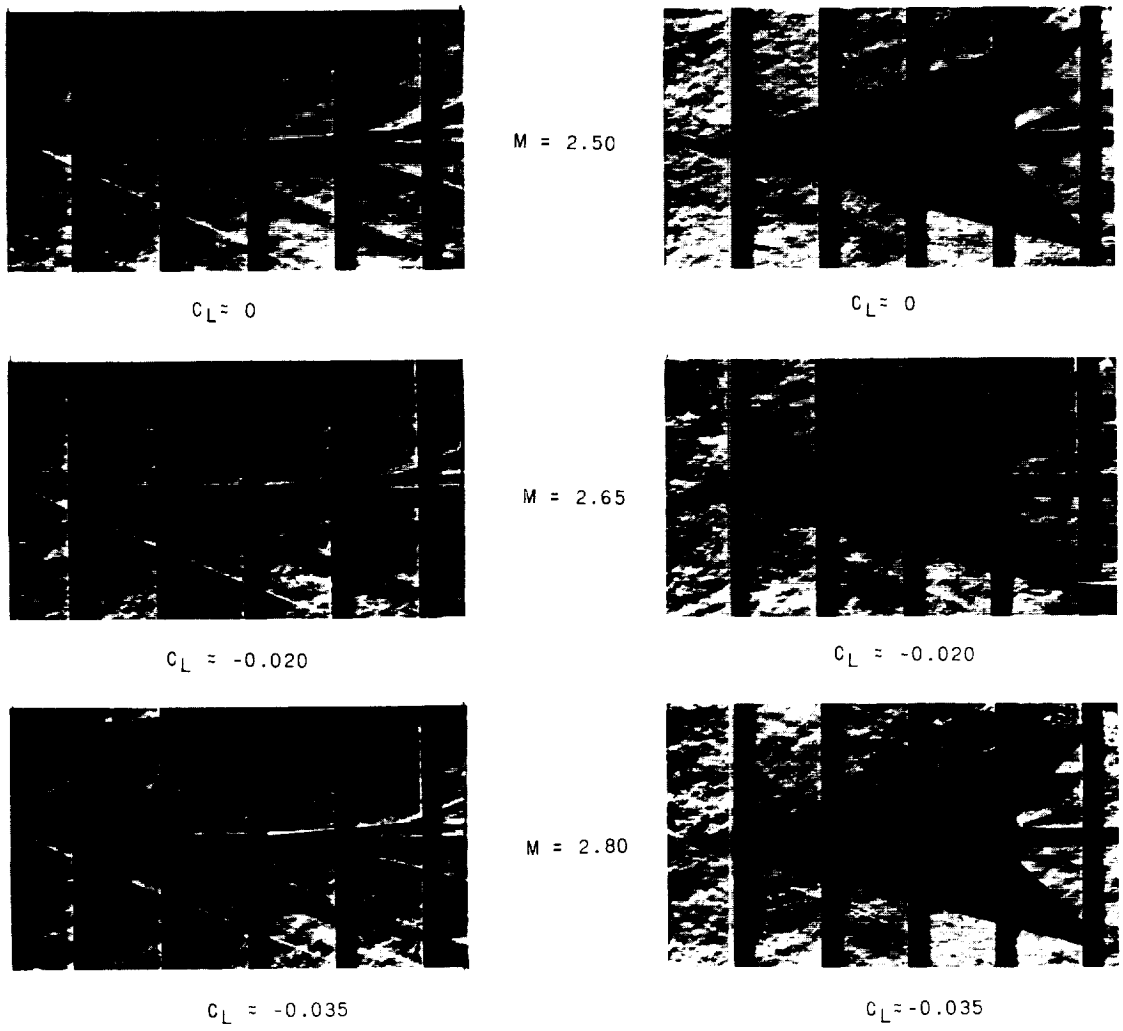

(b) Concluded. L-59-214

Figure 6.- Concluded

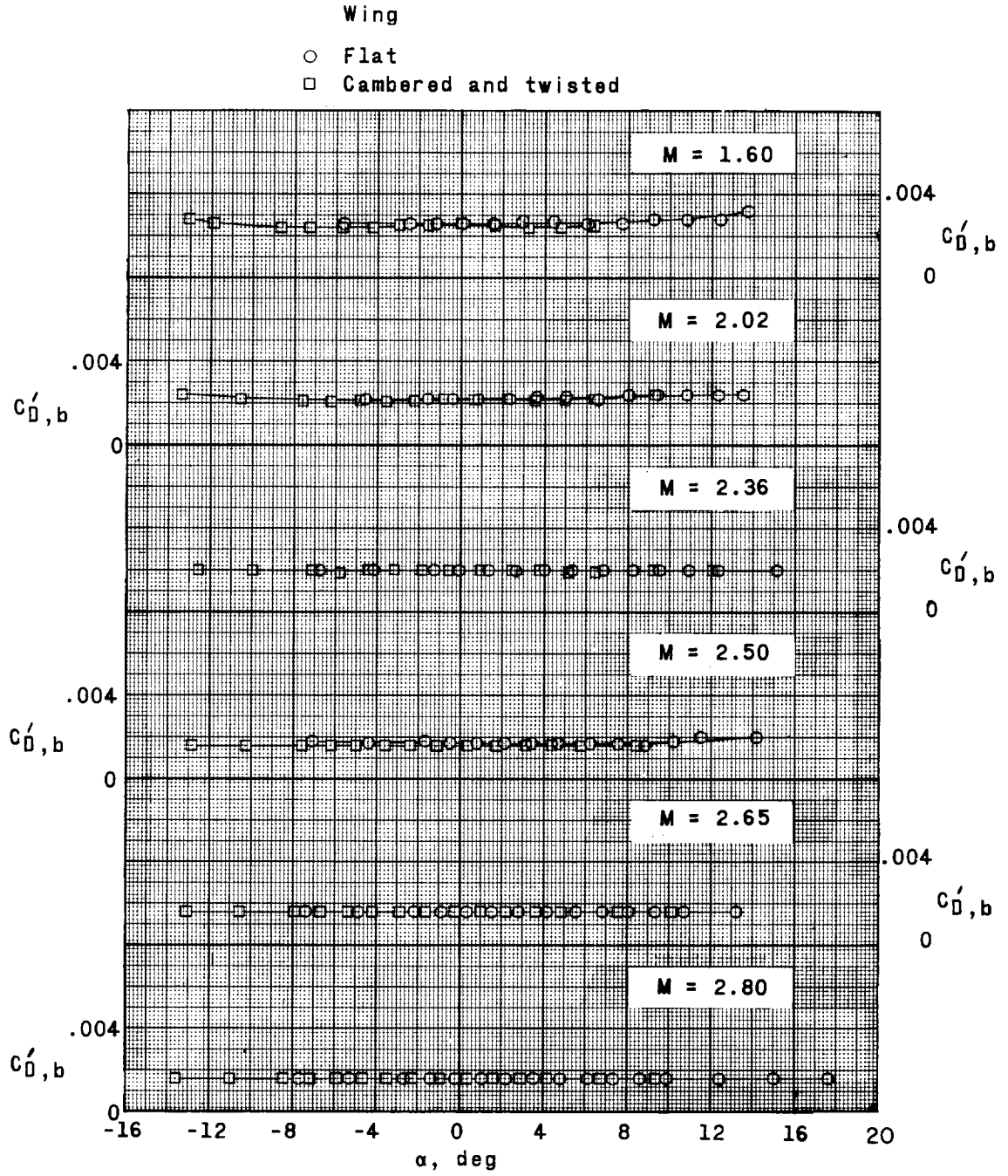

Figure 7.- Variation of base drag coefficient with angle of attack for various Mach numbers.

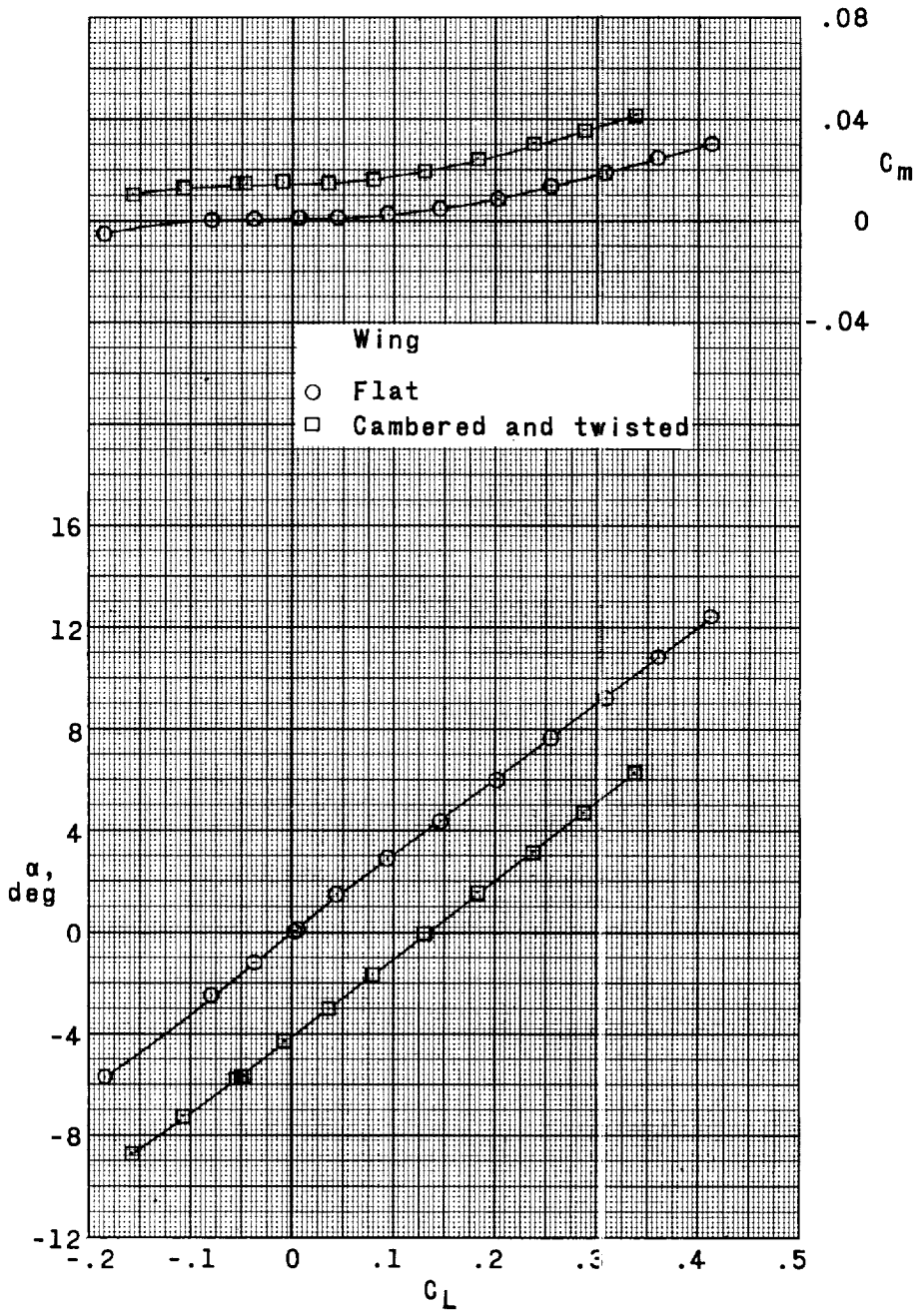

(a) M = 1.60.

Figure 8.- Aerodynamic characteristics in pitch for the arrow-wing models.

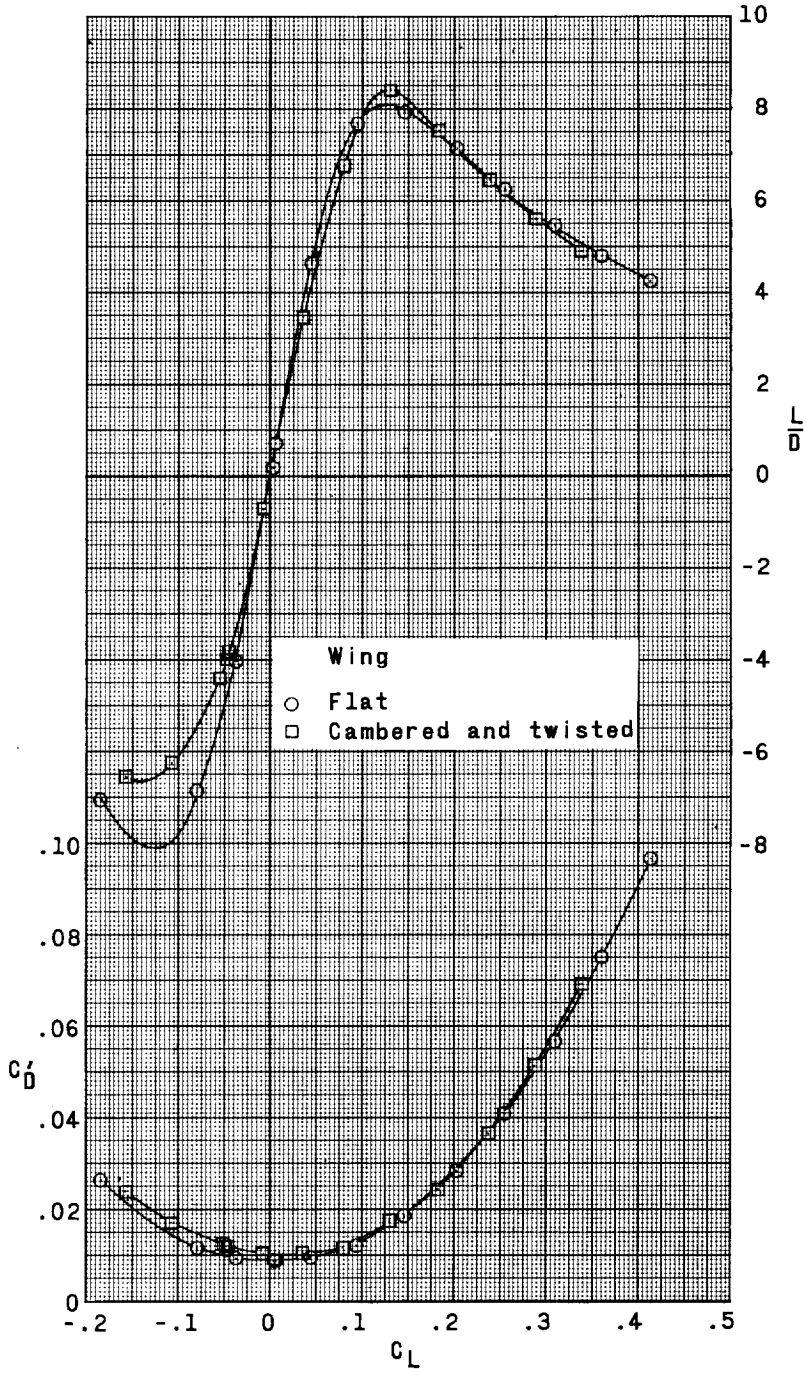

(a) Concluded.

Figure 8.- Continued.

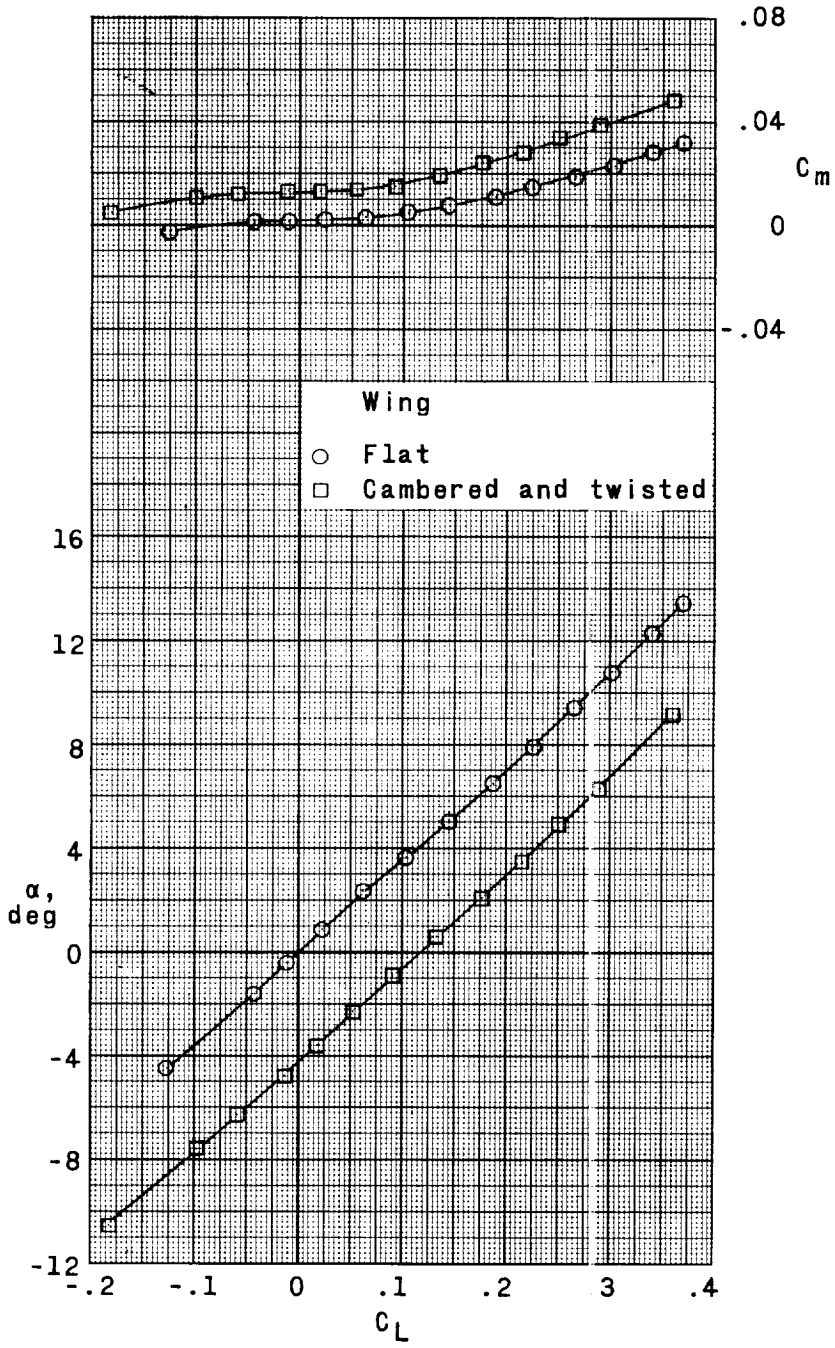

(b) M = 2.02.

Figure 8.- Continued.

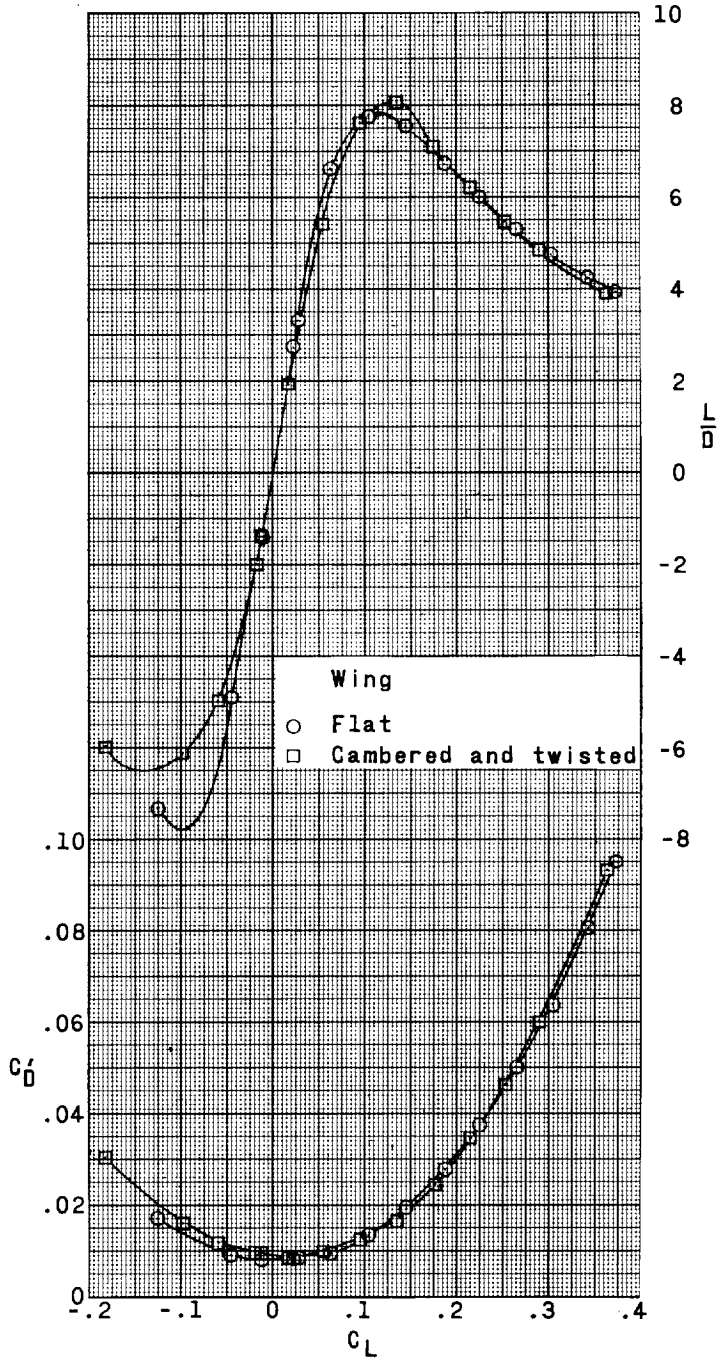

(b) Concluded.

Figure 8.- Continued.

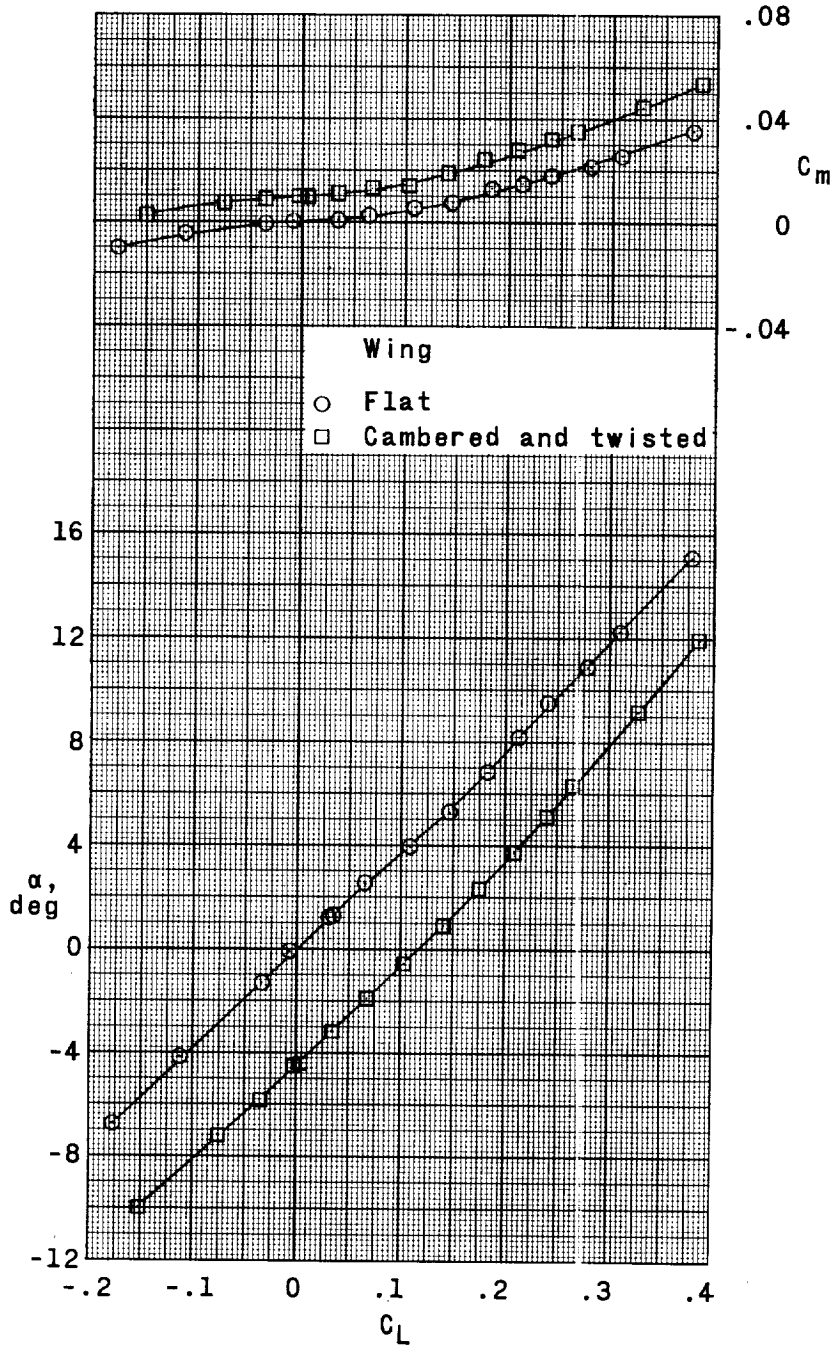

L-369

(c) M = 2.36.

Figure 8.- Continued.

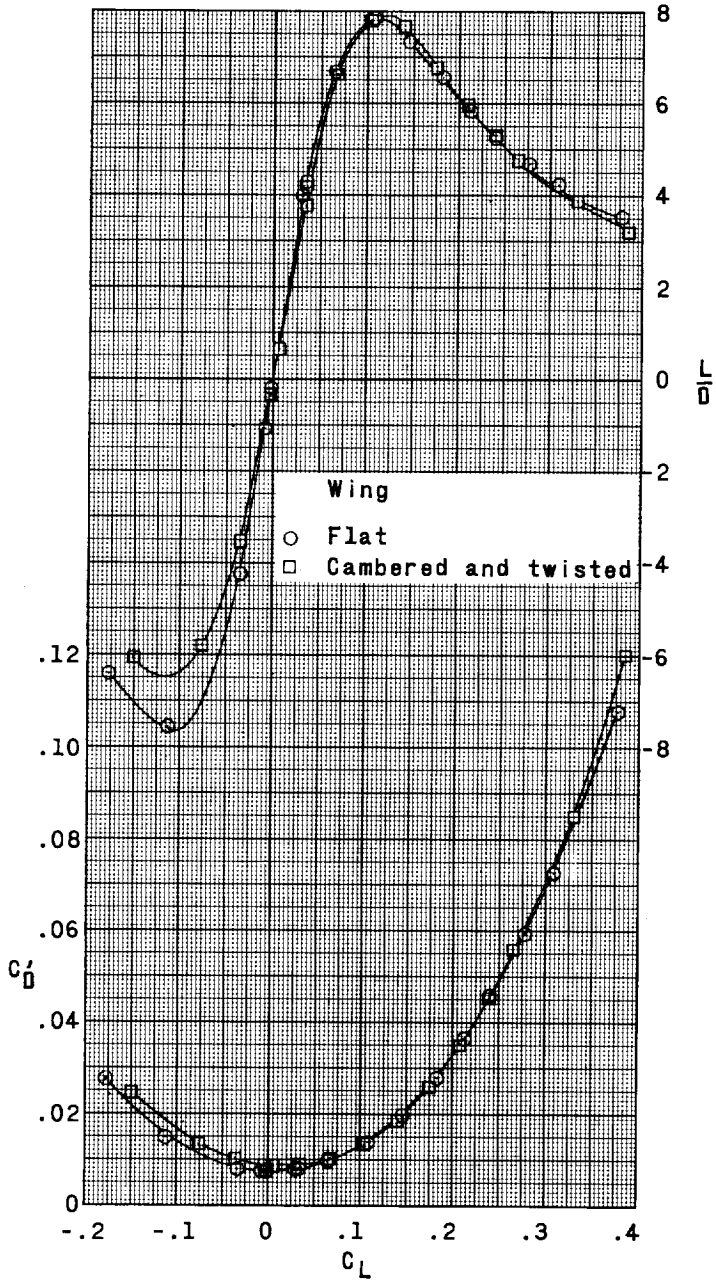

(c) Concluded.

Figure 8.- Continued.

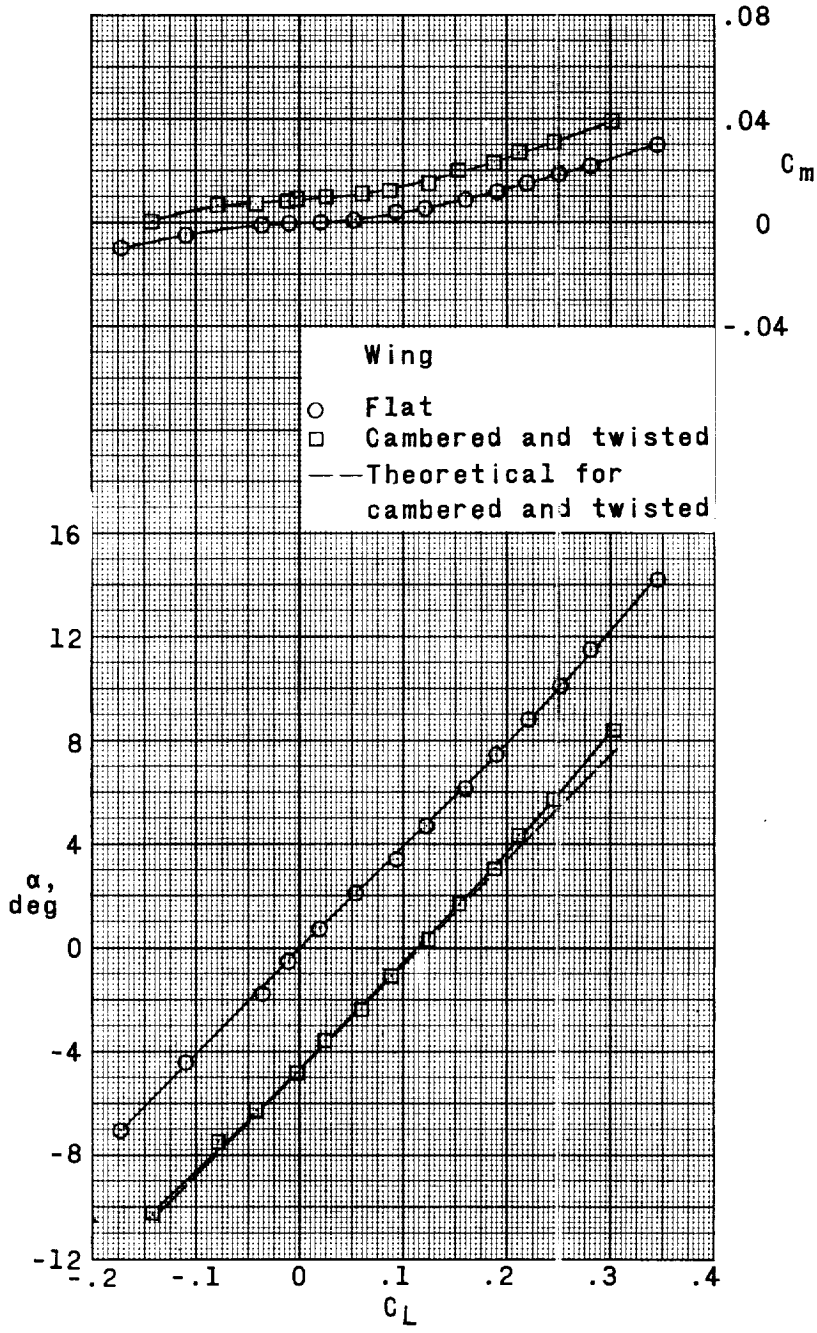

(d) M = 2.50.

Figure 8.- Continued.

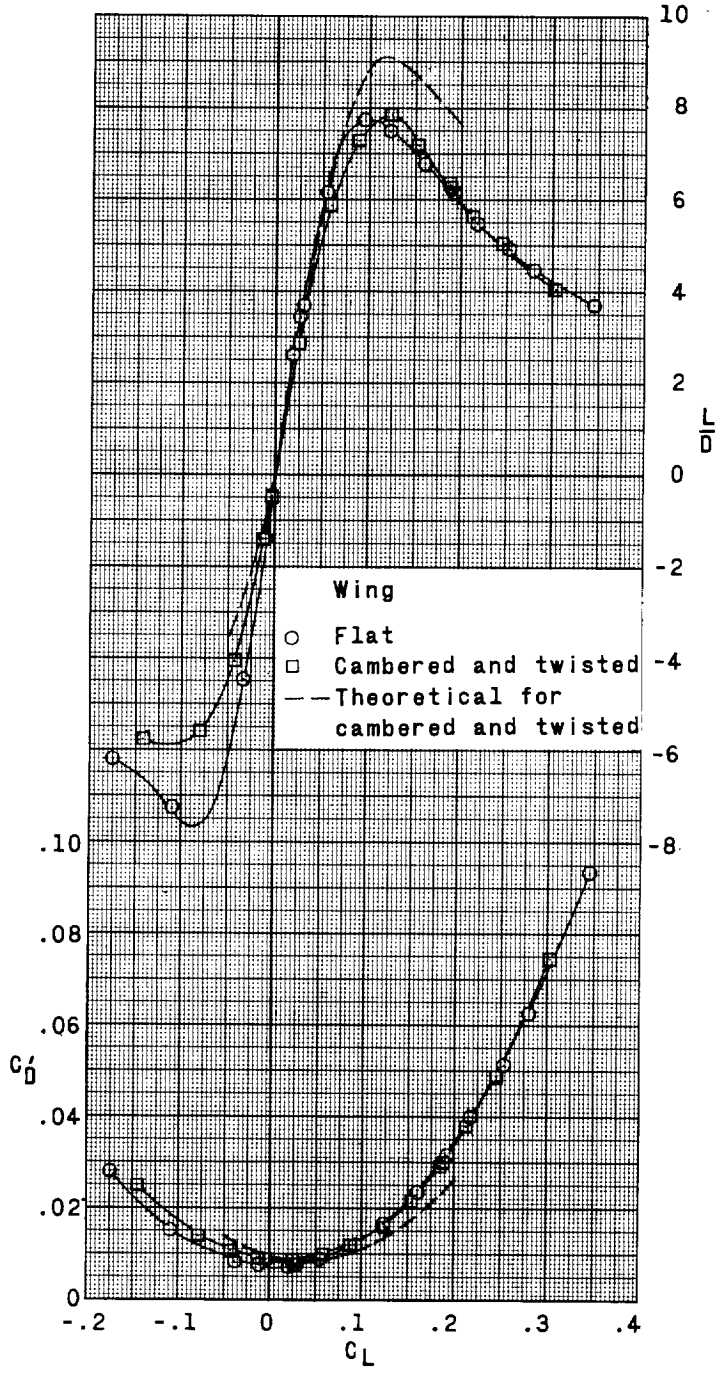

(d) Concluded.

Figure 8.- Continued.

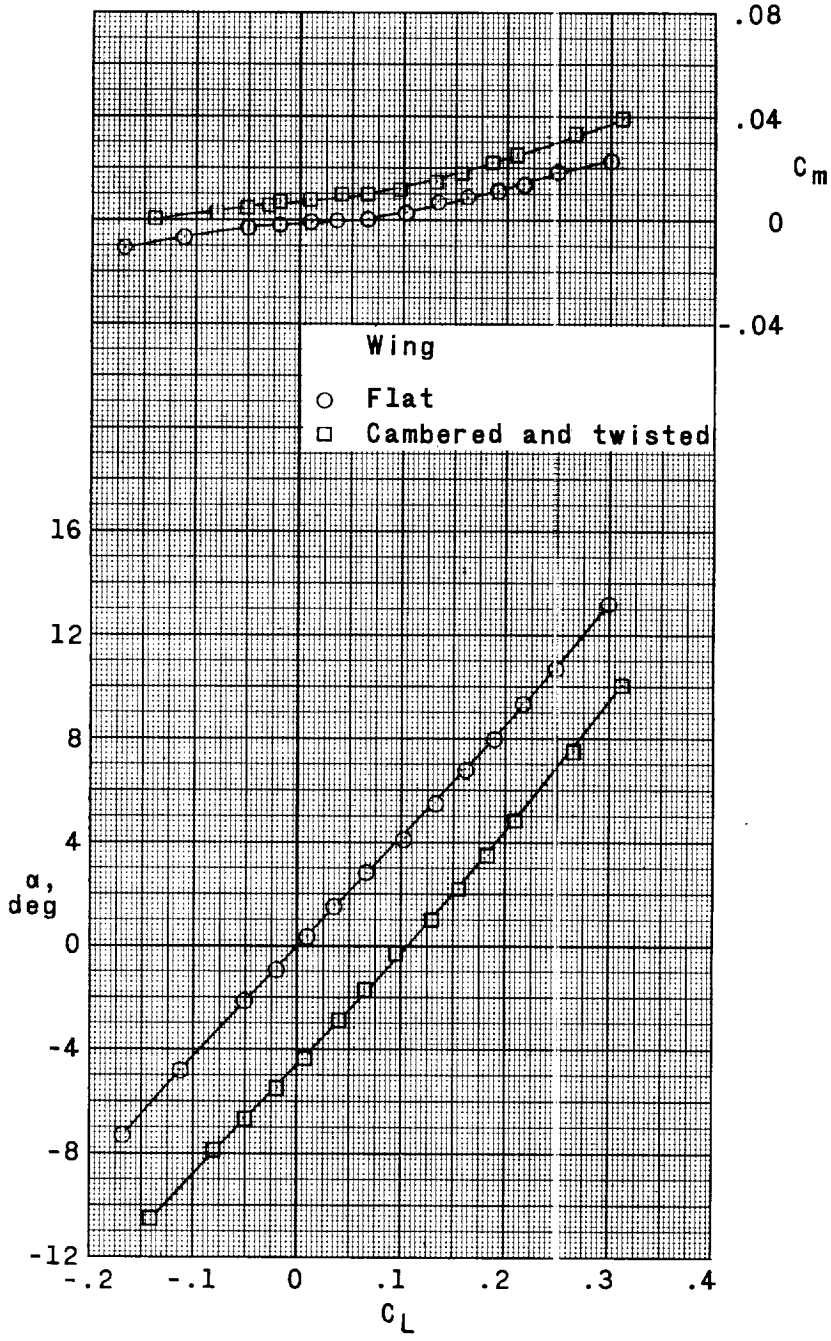

(e) M = 2.65.

Figure 8.- Continued.

L-369

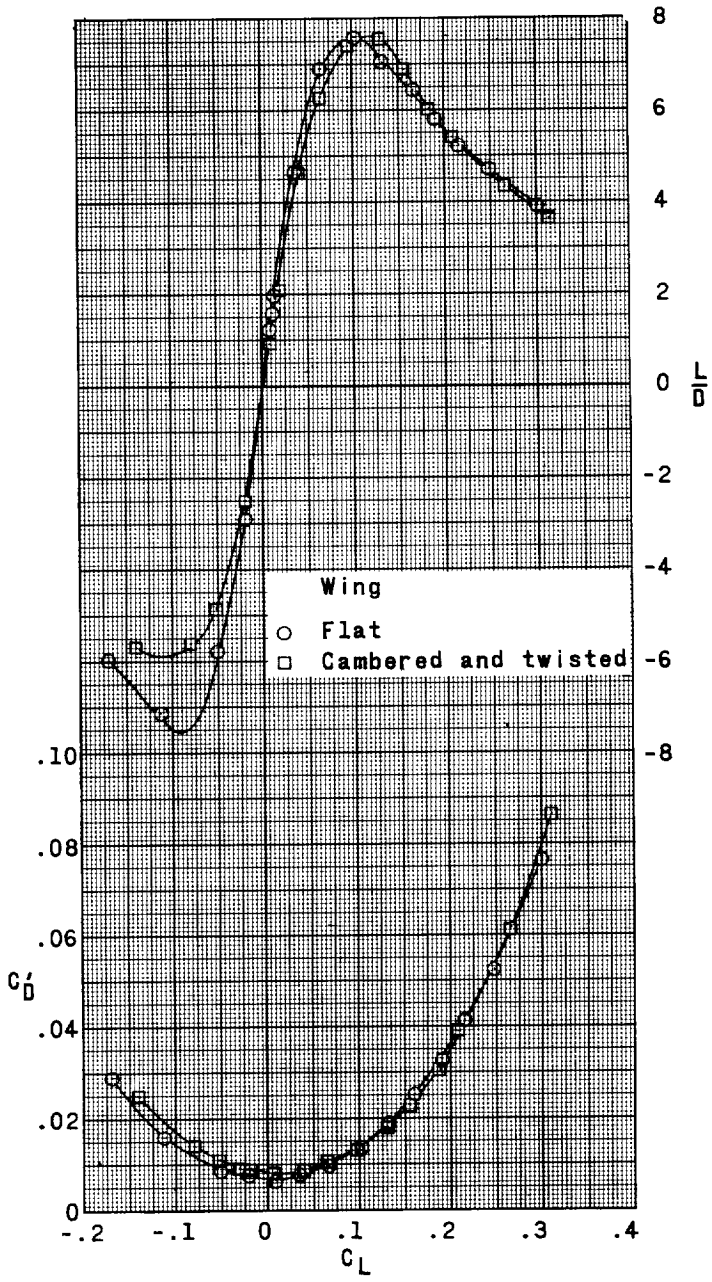

(e) Concluded.

Figure 8.- Continued.

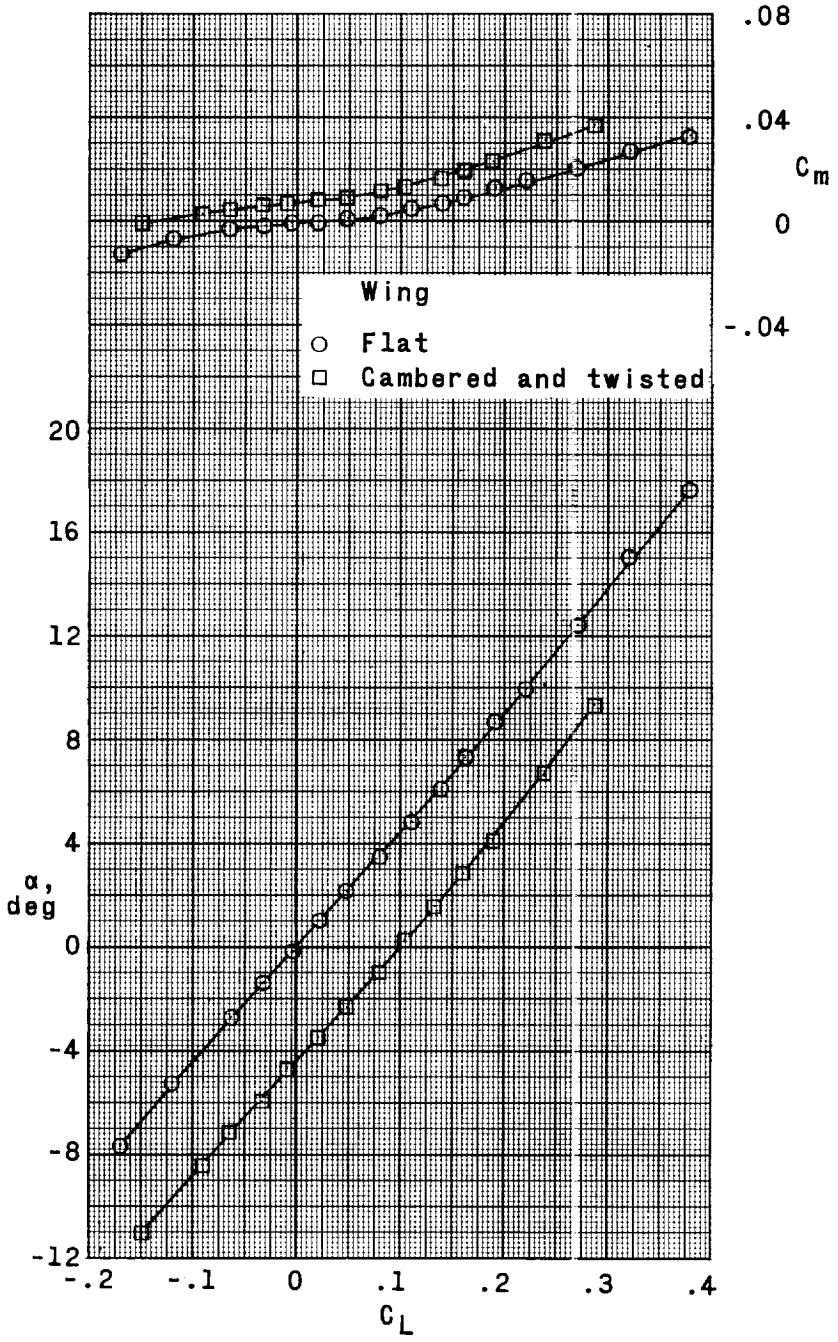

(f) M = 2.80.

Figure 8.- Continued.

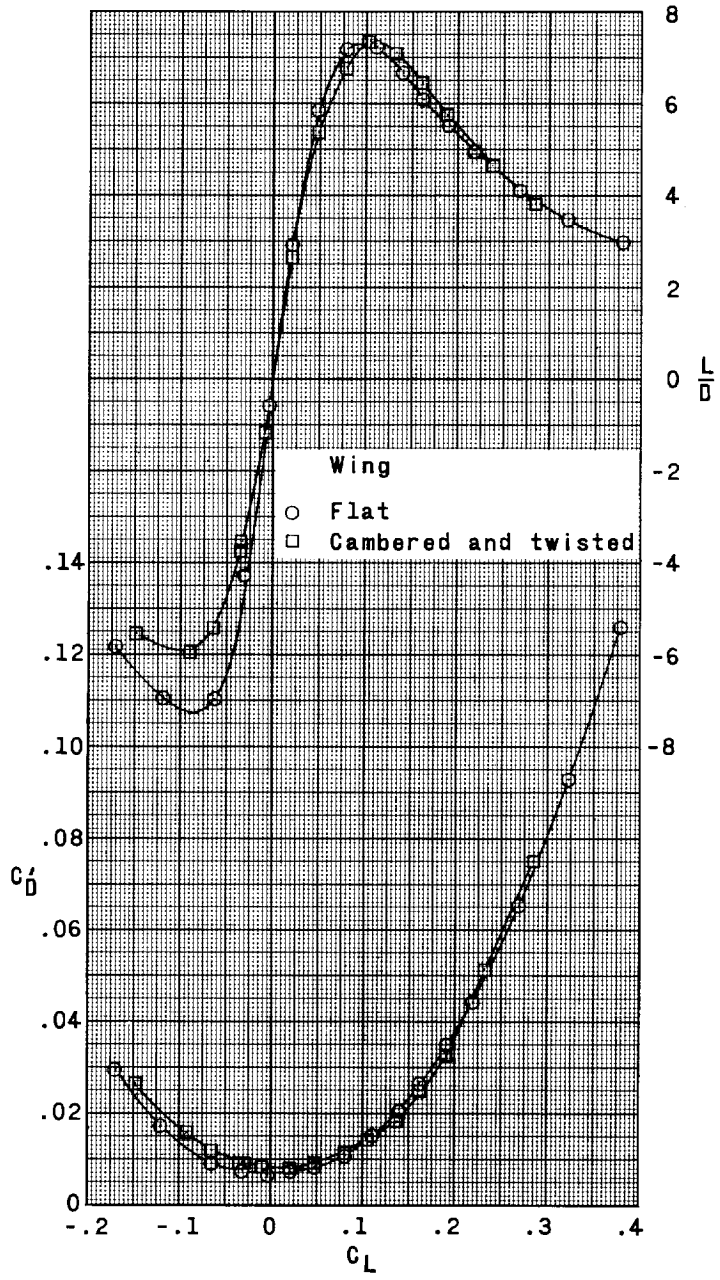

(f) Concluded.

Figure 8.- Concluded.

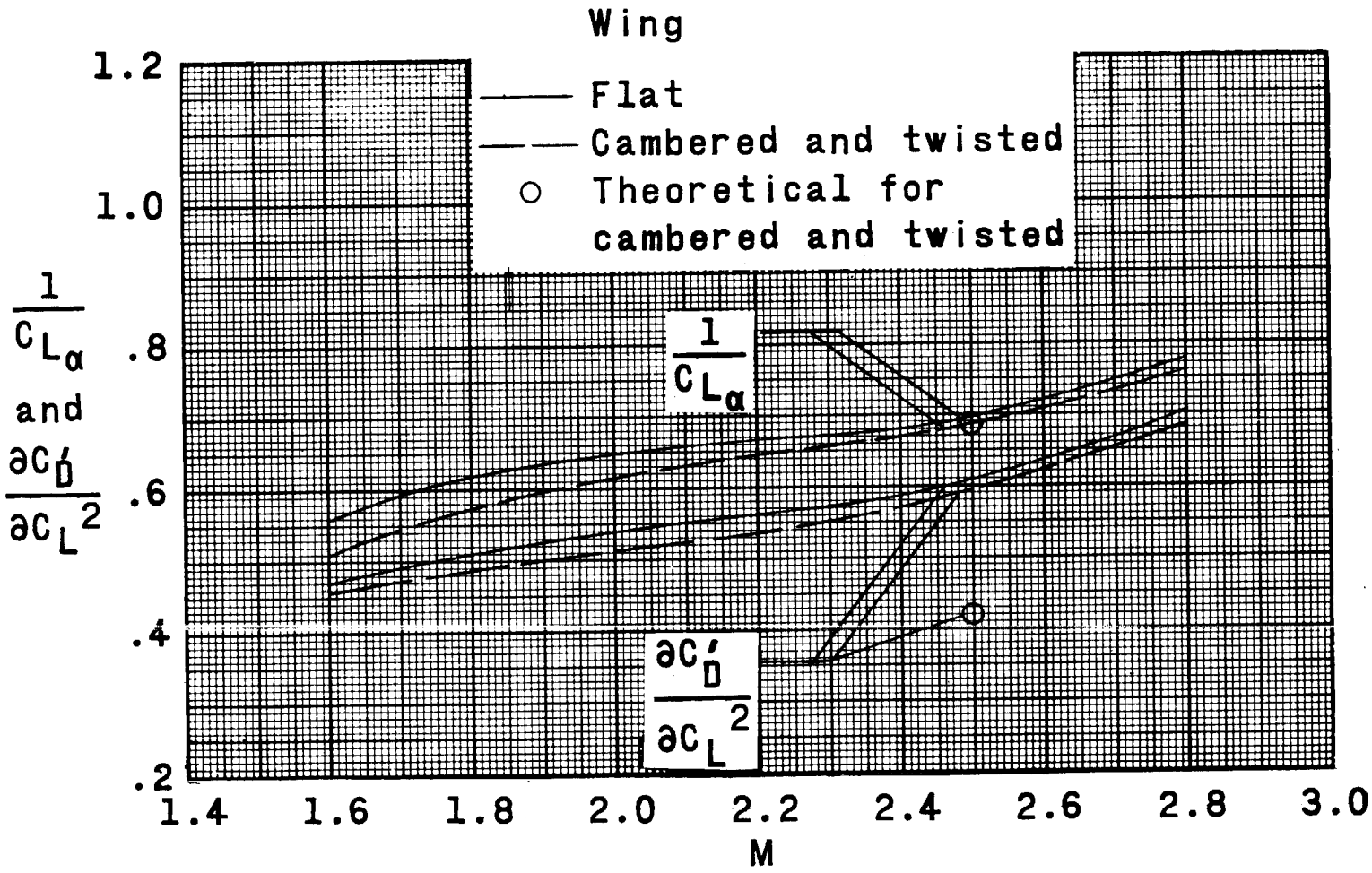

Figure 9.- Comparison of variation of $1/C_{L_\alpha}$ and $\partial C_D'/\partial C_L^2$ with Mach number for the arrow-wing models.

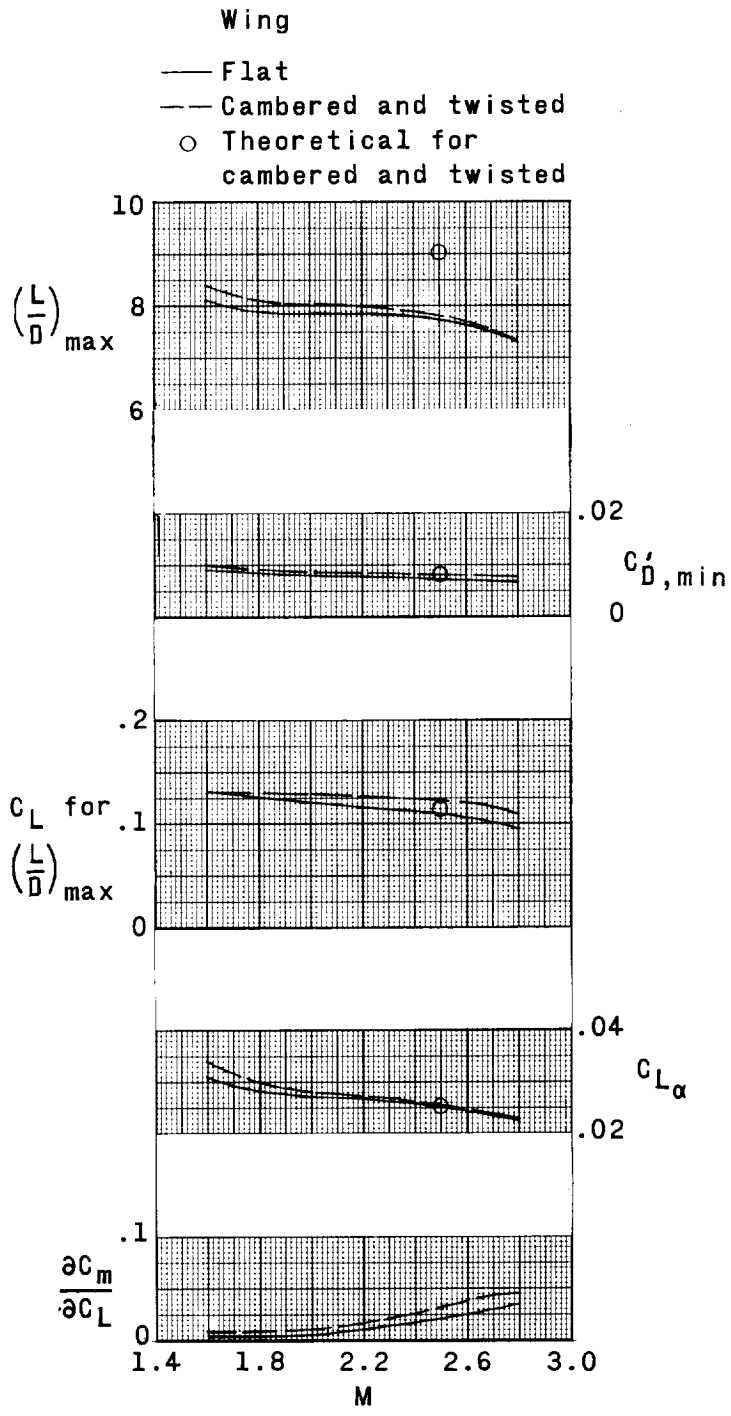

Figure 10.- Summary of longitudinal characteristics of the arrow-wing models.

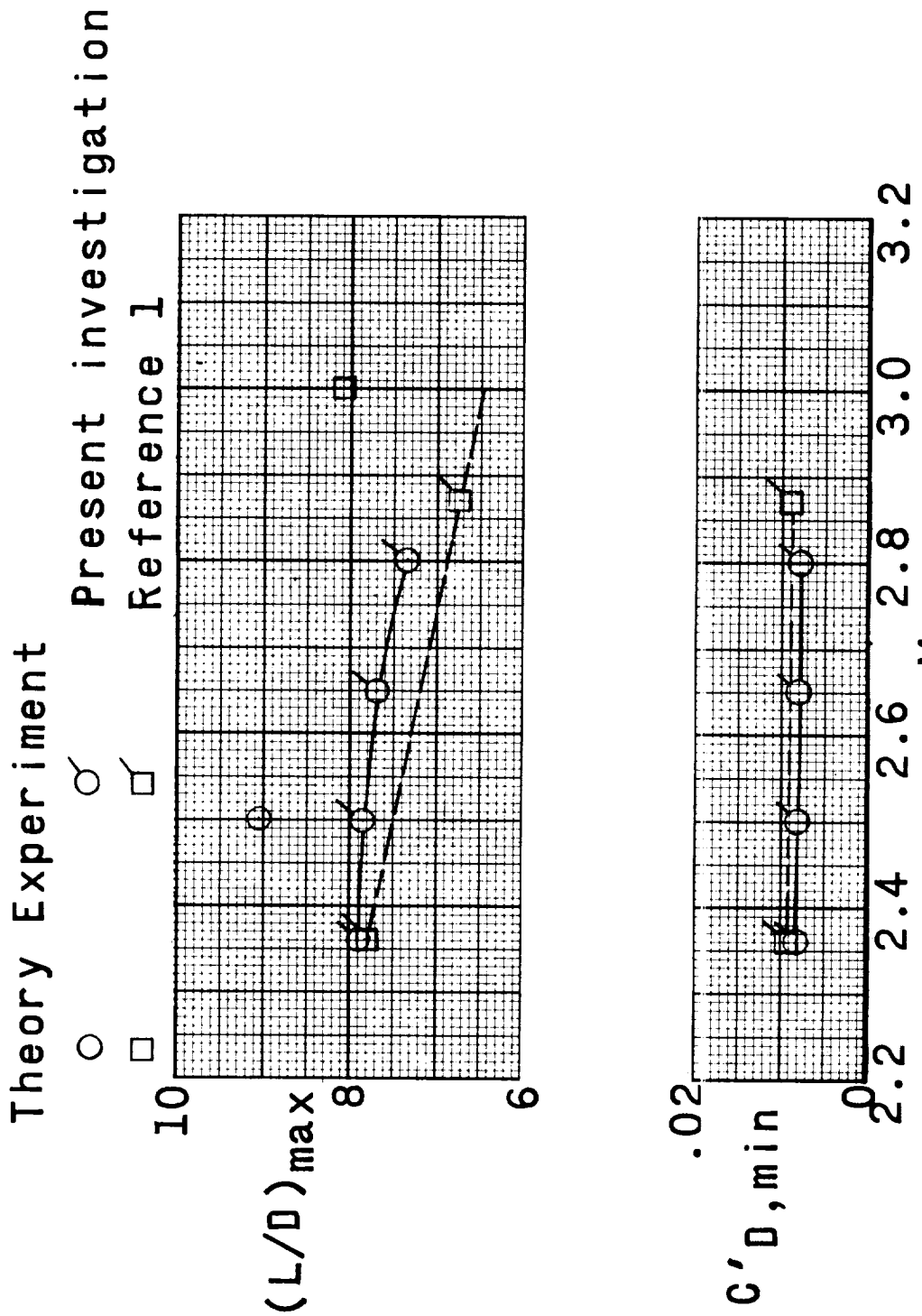

Figure 11.- Comparison of variation of $C'_{D,min}$ and $(L/D)_{max}$ with Mach number of cambered and twisted arrow wings. Fixed transition.